Polynuclear Nickel(II) Complexes: Preparation, Characterization, Magnetic Properties, and Quantum-Chemical Study of $[Ni_5(OH)(Rbta)_5(acac)_4(H_2O)_4]$ (RbtaH = Benzotriazole and 5,6-Dimethylbenzotriazole)

Vasilis Tangoulis, Catherine P. Raptopoulou, and Aris Terzis*

Institute of Materials Science, NCSR Demokritos, 153 10 Aghia Paraskevi Attikis, Greece

Evangelos G. Bakalbassis*

Laboratory of Applied Quantum Chemistry, Department of General and Inorganic Chemistry, Faculty of Chemistry, Aristotle University of Thessaloniki, 540 06 Thessaloniki, Greece

Eleanna Diamantopoulou and Spyros P. Perlepes*

Department of Chemistry, University of Patras, 265 00 Patras, Greece

Received November 7, 1997

The preparation and properties are described of two related Ni^{II}_5 clusters. The reactions of $[Ni(acac)_2(H_2O)_2]$ (acacH = acetylacetone) with benzotriazole (btaH) and 5,6-dimethylbenzotriazole (5,6diMebtaH) in refluxing Me_2CO in the presence of H_2O leads to the isolation of $[Ni_5(OH)(bta)_5(acac)_4(H_2O)_4]$ (**1**) and $[Ni_5(OH)(5,6diMebta)_5(acac)_4(H_2O)_4]$ (**2**) in 70−75 and 40−50% yields, respectively. Complex **1**·$4Me_2CO$·$0.5C_6H_{14}$ crystallizes in the triclinic space group $P\bar{1}$ with (at 25 °C) $a = 13.885(1)$ Å, $b = 12.013(1)$ Å, $c = 25.611(2)$ Å, $\alpha = 89.02(1)°$, $\beta = 104.76(2)°$, $\gamma = 111.78(1)°$, and $Z = 2$. Complex **2**·$4Me_2CO$ crystallizes in the monoclinic space group $C2/c$ with (at 25 °C) $a = 19.085(3)$ Å, $b = 20.142(3)$ Å, $c = 22.574(4)$ Å, $\beta = 103.30(1)°$, and $Z = 4$. The Ni^{II} assemblies of **1** and **2** are composed of a tetrahedral arrangement of four six-coordinate metal ions centered on the fifth. Each of the five $\eta^1{:}\eta^1{:}\eta^1{:}\mu_3$ benzotriazolate ligands spans an edge of the Ni_4 tetrahedron. The OH^- ion bridges three Ni^{II} ions and spans the sixth edge of the tetrahedron. A chelating $acac^-$ ion and a terminal H_2O molecule complete the coordination sphere of each peripheral metal. Variable-temperature magnetic susceptibility data (5.0−295 K), obtained for **1** and **2**, show antiferromagnetic interactions for both of them. The data are interpreted using a five-*J* model, which is based upon the hierarchy of algebras approach. Least-squares fitting of the data gives exchange parameters *J* for the interactions between the benzotriazolate-bridged peripheral Ni^{II} ions in the range from −3.9 to −10.7 cm^{-1}, and for those between the central ion and the peripheral ones in the range from −3.1 to −6.1 cm^{-1}; the *J* value for the interaction between the O-bridged peripheral nickels is −39.6 cm^{-1} for **1** and −43.2 cm^{-1} for **2**. Magnetization data are in line with an intermediate spin ground state [$S = 0$, $S = 1$] for both clusters. An orbital interpretation of the coupling is proposed.

Introduction

Magnets have fascinated humans for millenia, playing a crucial role in the development of modern science and technology.[1] Besides the current everyday uses of magnets, the "smart" switches, sensors, and transducers of tomorrow will undoubtedly benefit from magnetic materials. Considerable interest has therefore developed in devising ways of making new magnetic molecular materials exhibiting spontaneous magnetization below a critical temperature.[2]

The synthesis of molecules with large numbers of unpaired electrons is an area of great interest because it is widely recognized that such molecules are potential building blocks for molecular-based magnetic materials.[2,3] A number of strategies are currently available to access the latter.[4,5] The major difficulty (and a continuing challenge) is to develop the manipulative methodology to link molecular species with large spin values in the ground state in an appropriate manner so as to allow long-range ferro- and/or ferrimagnetic ordering in three dimensions. The search for molecules with large numbers of unpaired electrons is being pursued in both the organic[1,6] and inorganic areas. In the area of inorganic chemistry, a Mn^{II}_6 nitronyl nitroxide ring compound[7] with an $S = 12$ ground state

(1) Miller, J. S.; Epstein, A. J. *Angew. Chem., Int. Ed. Engl.* **1994**, *33*, 385.
(2) See, for example: *Magnetic Molecular Materials*; Gatteschi, D., Kahn, O., Miller, J. S., Palacio, F., Eds.; Kluwer: Dordrecht, The Netherlands, 1991.
(3) (a) Delfs, C. D.; Gatteschi, D.; Pardi, L. *Comments Inorg. Chem.* **1993**, *15*, 27. (b) Kahn, O.; Pei, Y.; Journaux, Y. Molecular Inorganic Magnetic Materials. In *Inorganic Materials*; Bruce, D. W., O'Hare, D., Eds.; Wiley: New York, 1992; pp 59−114.
(4) A brief review of these strategies has been recently given in ref 5.
(5) Tsai, H.-L.; Wang, S.; Folting, K.; Streib, W. E.; Hendrickson, D. N.; Christou, G. *J. Am. Chem. Soc.* **1995**, *117*, 2503.
(6) Nakamura, N.; Inoue, K.; Iwamura, H.; Fujioka, T.; Sawaki, Y. *J. Am. Chem. Soc.* **1992**, *114*, 1484.
(7) Caneschi, A.; Gatteschi, D.; Laugier, J.; Rey, P.; Sessoli, R.; Zanchini, C. *J. Am. Chem. Soc.* **1988**, *110*, 2795.

S0020-1669(97)01409-2 CCC: $15.00
Published on Web 06/02/1998

held the record for the highest spin multiplicity for several years. Recently synthesized $Mn^{II}_6Mn^{III}_4$ and $Fe^{III}_{17}/Fe^{III}_{19}$ clusters show $S = 12$ and $S \geq 33/2$ ground states, respectively.[8,9]

One of the key features for the observation of superparamagnetic behavior is the presence of a large magnetic anisotropy in the cluster.[10] Since nickel(II) is known to have a large single-ion zero-field splitting and often gives rise to ferromagnetic coupling, we decided to begin a new program directed toward preparation and magnetic characterization of high-nuclearity Ni^{II} clusters hoping to obtain some high-spin species. Although polynuclear nickel(II) complexes containing up to four metal atoms are not rare,[11] clusters with five,[12] six,[13] seven,[10,14a] eight,[15] or more[14] nickel(II) atoms remain rare.

We recently communicated the structure and preliminary magnetic results of the novel complex $[Ni_5(OH)(bta)_5(acac)_4(H_2O)_4]\cdot 4Me_2CO\cdot 0.5C_6H_{14}$ (**1**·$4Me_2CO\cdot 0.5C_6H_{14}$; btaH = benzotriazole, **I**; acacH = acetylacetone).[16] In the present article

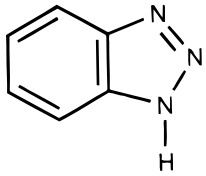

I, btaH

we report a significant extension of this work, including the full characterization of **1**, the interpretation of its magnetic properties in more detail, and the preparation, single-crystal X-ray structure, and magnetic study of the new analogous complex $[Ni_5(OH)(5,6diMebta)_5(acac)_4(H_2O)_4]\cdot 4Me_2CO$ (**2**·$4Me_2CO$; 5,6diMebtaH = 5,6-dimethylbenzotriazole) which has a higher symmetry. To the best of our knowledge, no studies have been reported for nonlinear pentanuclear magnetic Ni^{II} clusters. Moreover, it is the first time that a solution for a Hamiltonian involving five different exchange parameters as well as its application on very low symmetry magnetic systems is attempted. In particular, we want to show how it is possible to obtain a detailed understanding of the structural basis of the magnetic properties of these two asymmetric Ni_5 clusters using the hierarchy of algebras approach, within the spin Hamiltonian formalism. An orbital interpretation of the magnetic coupling based upon the results of quantum-chemical calculations is also presented.

Experimental Section

Materials. All manipulations were performed under aerobic conditions using materials as received (Aldrich Co.); water was distilled in-house. The compound $[Ni(acac)_2(H_2O)_2]$ was prepared as described elsewhere.[17]

Physical Measurements and Theoretical Calculations. C, H, and N analyses were conducted by the University of Ioannina, Greece, microanalytical service, and nickel analysis was carried out by EDTA titration. Infrared spectra (4000−500 cm^{-1}) were recorded on a Perkin-Elmer 16 PC infrared spectrometer with samples prepared as KBr pellets. Far-infrared spectra (500−100 cm^{-1}) were recorded on a Bruker IFS 113v FT spectrometer with a liquid nitrogen-cooled MCT detector using polyethylene pellets. Solid-state (diffuse reflectance, 800−300 nm) electronic spectra were recorded on a Varian, Cary 3 instrument. Magnetic susceptibility measurements were carried out on polycrystalline samples of **1** and **2** in the 295−5.0 K temperature range using a Quantum Design SQUID susceptometer. The applied magnetic field was 6000 G. The experimental magnetic susceptibilities were corrected for the diamagnetic response using Pascal's constants. Least-squares computer fittings of the susceptibility data were performed with the multidimensional minimization package MERLIN/MCL;[18] several optimization techniques such as the BFGS algorithm, the Conjugate Gradient algorithm, etc. have also been used. Solid-state EPR spectra were recorded on a Bruker ER 200D-SRC X-band spectrometer, equipped with an Oxford ESR 9 cryostat, in the temperature range 295−4.2 K. CNDO calculations were performed on a Macintosh Classic personal computer using QCPE's program QMAC019.[19]

Safety Note! *Benzotriazoles and benzotriazolate complexes are potentially explosive, and caution should be exercised when dealing with such derivatives.* However, the small quantities used in this study were not found to present a hazard.

$[Ni_5(OH)(bta)_5(acac)_4(H_2O)_4]\cdot 4Me_2CO\cdot 0.5C_6H_{14}$ (1·$4Me_2CO\cdot 0.5C_6H_{14}$). $[Ni(acac)_2(H_2O)_2]$ (0.30 g, 1.02 mmol) was partially dissolved in a mixture of Me_2CO (25 mL) and H_2O (0.5 mL) with stirring and reflux to give a pale green solution and undissolved material. To this slurry was added a solution of btaH (0.12 g, 1.02 mmol) in Me_2CO (5 mL), which caused a slow color change to blue. The reflux was continued for a further 15 min. The resulting solution was filtered and left undisturbed at ambient temperature for 48 h. A small quantity of a sky-blue precipitate (**1a**) was obtained and collected by filtration. Layering of *n*-hexane into the dark blue filtrate gave blue prisms of

(8) (a) Goldberg, D. P.; Caneschi, A.; Delfs, C. D.; Sessoli, R.; Lippard, S. J. *J. Am. Chem. Soc.* **1995**, *117*, 5789. (b) Barra, A. L.; Caneschi, A.; Gatteschi, D.; Sessoli, R. *J. Am. Chem. Soc.* **1995**, *117*, 8855.

(9) Powell, A. K.; Heath, S. L.; Gatteschi, D.; Pardi, L.; Sessoli, R.; Spina, G.; Giallo, F. D.; Pieralli, F. *J. Am. Chem. Soc.* **1995**, *117*, 2491.

(10) Fallah M. S. E.; Rentschler, E.; Caneschi, A.; Sessoli, R.; Gatteschi, D. *Inorg. Chem.* **1996**, *35*, 3723.

(11) (a) Halcrow, M. A.; Sun, J.-S.; Huffman, J. C.; Christou, G. *Inorg. Chem.* **1995**, *34*, 4167 and references therein. (b) Ribas, J.; Monfort, M.; Costa, R.; Solans, X. *Inorg. Chem.* **1993**, *32*, 659. (c) Ballester, L.; Coronado, E.; Gutierrez, A.; Monge, A.; Perpinan, M. F.; Pinilla, E.; Rico, T. *Inorg. Chem.* **1992**, *31*, 2053. (d) Kruger, P. E.; Fallon, G. D.; Moubaraki, B.; Murray, K. S. *J. Chem. Soc., Chem. Commun.* **1992**, 1726. (e) Paap, F.; Bouwman, E.; Driessen, W. L.; De Graaff, R. A. G.; Reedijk, J. *J. Chem. Soc., Dalton Trans.* **1985**, 737. (f) Gladfelter, W. L.; Lynch, M. W.; Schaefer, W. P.; Hendrickson, D. N.; Gray, H. B. *Inorg. Chem.* **1981**, 20, 2390. (g) Bertrand, J. A.; Ginsberg, A. P.; Kaplan, R. I.; Kirkwood, C. E.; Martin, R. L.; Sherwood, R. C. *Inorg. Chem.* **1971**, *10*, 240. (h) Murray, K. S. *Adv. Inorg. Chem.* **1995**, *43*, 261.

(12) (a) Shieh, S.-J.; Chou, C.-C.; Lee, G.-H.; Wang, C.-C.; Peng, S.-M. *Angew. Chem., Int. Ed. Engl.* **1997**, *36*, 56. (b) Velazquez, C. S.; Baumann, T. F.; Olmstead, M. M.; Hope, H.; Barrett, A. G. M.; Hoffman, B. M. *J. Am. Chem. Soc.* **1993**, *115*, 9997. (c) Fenske, D.; Krautscheid, H.; Muller, M. *Angew. Chem., Int. Ed. Engl.* **1992**, *31*, 321. (d) Koo, B.-K.; Block, E.; Kang., H.; Liu, S.; Zubieta, J. *Polyhedron* **1988**, *7*, 1397. (e) Kriege, M.; Henkel, G. *Z. Naturforsch.* **1987**, *42B*, 1121. (f) Finney, A. J.; Hitchman, M. A.; Raston, C. L.; Rowbottom, G. L.; White, A. H. *Aust. J. Chem.* **1981**, *34*, 2139.

(13) (a) Cornia, A.; Fabretti, A. C.; Gatteschi, D.; Palyi, G.; Rentschler, E.; Shchegolikhina, O. I.; Zhdanov, A. A. *Inorg. Chem.* **1995**, *34*, 5383 and references therein. (b) Lewis, G. E.; Kraihanzel, C. S. *Inorg. Chem.* **1983**, *22*, 2895. (c) Cotton, F. A.; Winquist, B. H. C. *Inorg. Chem.* **1969**, *8*, 1304. (d) Woodward, P.; Dahl, L. F.; Abel, E. W.; Crosse, B. C. *J. Am. Chem. Soc.* **1965**, *87*, 5251.

(14) (a) Brechin, E. K.; Harris, S. G.; Parsons, S.; Winpenny, R. E. P. *Angew. Chem., Int. Ed. Engl.* **1997**, *36*, 1967. (b) Brechin, E. K.; Graham, A.; Harris, S. G.; Parsons, S.; Winpenny, R. E. P. *J. Chem. Soc., Dalton Trans.* **1997**, 3405. (c) Blake, A. J.; Brechin, E. K.; Codron, A.; Gould, R. O.; Grant, C. M.; Parsons, S.; Rawson, J. M.; Winpenny, R. E. P. *J. Chem. Soc., Chem. Commun.* **1995**, 1983. (d) Blake, A. J.; Grant, C. M.; Parsons, S.; Rawson, J. M.; Winpenny, R. E. P. *J. Chem. Soc., Chem. Commun.* **1994**, 2363.

(15) (a) Faus, J.; Lloret, F.; Julve, M.; Clemente-Juan, J. M.; Munoz, M. C.; Solans, X.; Font-Bardia, M. *Angew. Chem., Int. Ed. Engl.* **1996**, *35*, 1485. (b) Dance, I. G.; Scudder, M. L.; Secomb, R. *Inorg. Chem.* **1985**, *24*, 1201.

(16) Bakalbassis, E. G.; Diamantopoulou, E.; Perlepes, S. P.; Raptopoulou, C. P.; Tangoulis, V.; Terzis, A.; Zafiropoulos, Th. F. *J. Chem. Soc., Chem. Commun.* **1995**, 1347.

(17) Charles, R. G.; Pawlikowski, M. A. *J. Phys. Chem.* **1958**, *62*, 440.

(18) Chassapis, C. S.; Papageorgiou, D. G.; Lagaris, I. E. *Comput. Phys. Commun.* **1989**, *52*, 223, 241.

(19) Sigalas, M. P.; Katsoulos, G. A. QMAC019, CNDEX, Program for CNDO/INDO Reactivity Indices Calculations. *QCPE Bull.* **1994**, *14*, 4.

1·4Me_2CO·0.5C_6H_{14}. Typical yields are in the 70−75% range. A sample for crystallography was kept in contact with the mother liquor to prevent interstitial solvent loss. Collection of the crystals by filtration, washing with Et_2O, and drying in vacuo leads to the unsolvated form. Anal. Calcd (found) for $C_{50}H_{57}Ni_5N_{15}O_{13}$: C, 43.84 (43.6); H, 4.20 (4.3); N, 15.34 (15.0); Ni, 21.43 (21.8). IR data (KBr pellet, cm^{-1}) for **1**: 3590 (m), 3405 (s, br), 3072 (w), 3050 (w), 3020 (w), 2996 (w), 2916 (w), 1594 (vs), 1518 (vs), 1460 (m), 1402 (vs), 1364 (sh), 1262 (m), 1212 (m), 1200 (m), 1148 (w), 1130 (vw), 1092 (w), 1018 (s), 992 (m), 926 (s), 850 (w), 792 (m), 750 (s), 700 (w), 656 (w), 642 (w), 574 (m), 562 (m). Far-IR data (polyethylene pellet, cm^{-1}): 488 (w), 480 (w), 461 (w, br), 438 (m), 417 (s), 381 (w, br), 344 (m), 319 (sh), 299 (s), 282 (s), 255 (w, br), 240 (w), 225 (m), 198 (sh), 152 (w), 148 (w). Solid-state (diffuse reflectance) electronic spectrum (λ_{max}, nm): 725 (sh), 615, 390, 365. Product **1a** analyzes satisfactorily for $Ni_5(bta)_6(acac)_4$. Anal. Calcd (found) for $C_{56}H_{52}Ni_5N_{18}O_8$: C, 48.08 (48.2); H, 3.75 (3.8); N, 18.03 (17.7); Ni, 20.99 (21.5).

[Ni_5(OH)(5,6diMebta)$_5$(acac)$_4$(H_2O)$_4$]·4Me_2CO (2·4Me_2CO). To a stirred blue-green slurry of [Ni(acac)$_2$(H_2O)$_2$] (0.30 g, 1.02 mmol) in Me_2CO (21 mL) and H_2O (0.2 mL) was added a pale brown solution of 5,6diMebtaH (0.15 g, 1.02 mmol) in Me_2CO (4 mL) under reflux, which caused a rapid color change to olive green and complete dissolution of solid. The reaction mixture was refluxed for a further 15 min, and then allowed to cool slowly to ambient temperature and left undisturbed for 2 h. The resulting blue-green powder (**2a**) was collected by filtration. The blue-green filtrate was layered with *n*-hexane (50 mL) at ∼5 °C; after 2 weeks, blue-green crystals of the product were collected by filtration, washed with Et_2O (3 × 5 mL), and dried in air. Typical yields are in the 40−50% range (based on Ni). The crystals were found to lose solvent readily, and they were kept in the mother liquor until a suitable crystal had been found for X-ray crystallography. The latter established the formulation **2**·4Me_2-CO; the dried analysis sample analyzed for **2**. Anal. Calcd (found) for $C_{60}H_{77}Ni_{15}O_{13}$: C, 47.72 (48.0); H, 5.15 (5.0); N, 13.92 (13.7); Ni, 19.44 (20.5). IR data (KBr, cm^{-1}) for **2**: 3570 (m), 3388 (m, br), 3072 (w), 2970 (w), 2922 (w), 2858 (w), 1596 (vs), 1518 (vs), 1452 (m), 1402 (vs), 1290 (w), 1260 (w), 1212 (m), 1200 (sh), 1168 (w), 1090 (w), 1016 (m), 1008 (m), 992 (m), 856 (m), 826 (w), 758 (m), 656 (w), 574 (m), 506 (m). Far-IR data (polyethylene pellet, cm^{-1}): 470 (m), 443 (m, br), 415 (m), 382 (s), 360 (m), 331 (w), 273 (s, br), 265 (sh), 252 (sh), 235 (w), 219 (w), 183 (w), 146 (w, br). Solid-state (diffuse reflectance) electronic spectrum (λ_{max}, nm): 740 (sh), 635, 385 (sh), 357. Product **2a** appears to be slightly hygroscopic; this has made obtaining good analytical data difficult. An analysis sample gave results consistent with Ni_5(5,6diMebta)$_6$(acac)$_4$·H_2O. Anal. Calcd (found) for $C_{68}H_{78}Ni_5N_{18}O_9$: C, 51.52 (51.7); H, 4.97 (5.0); N, 15.91 (15.7); Ni, 18.52 (19.2).

X-ray Crystallography. A blue prismatic crystal of **1**·4Me_2-CO·0.5C_6H_{14} with approximate dimensions 0.15 × 0.35 × 0.55 mm and a blue-green crystal of **2**·4Me_2CO (0.15 × 0.30 × 0.50 mm) were mounted in capillary filled with drops of mother liquid. Diffraction measurements of **1**·4Me_2CO·0.5C_6H_{14} were made on a P21 Nicolet diffractometer using Zr-filtered Mo radiation, while for **2**·4Me_2CO a Crystal Logic Dual Goniometer diffractometer using graphite-monochromated Mo radiation was employed. Complete crystal data and parameters for data collection for complex **2**·4Me_2CO are reported in Table 1. In both cases, the unit cell dimensions were determined and refined by using the angular settings of 25 automatically centered reflections in the range $11 < 2\theta < 23°$. Intensity data were recorded using a $\theta-2\theta$ scan. For of **1**·4Me_2CO·0.5C_6H_{14}: $2\theta(max) = 46.4°$, scan speed 3.0°/min, scan range 2.5° plus $\alpha_1\alpha_2$ separation; for **2**·4Me_2-CO: $2\theta(max) = 45.0°$, scan speed 2.0°/min, scan range 2.5° plus $\alpha_1\alpha_2$ separation. Three standard reflections monitored every 97 reflections showed less than 3% fluctuation and no decay. Lorentz, polarization, and ψ scan absorption corrections were applied using Crystal Logic software.

Symmetry equivalent data of **1**·4Me_2CO·0.5C_6H_{14} and **2**·4Me_2CO were averaged with $R = 0.0174$ and 0.0241, respectively, to give 10 713 and 5520 independent reflections from a total 11 263 and 5714 collected. The structures were solved by direct methods using the programs SHELXS-86[20a] and refined by full-matrix least-squares techniques on F^2 with SHELX-93[20b] using 10 709 (**1**·4Me_2CO·0.5C_6H_{14}) and 5520 (**2**·4Me_2CO) reflections and refining 1030 and 653 parameters, respectively. For **1**·4Me_2CO·0.5C_6H_{14}, all hydrogen atoms of the methyl groups of the $acac^-$ ligands were introduced at calculated positions as riding on bonded atoms, those of the Me_2CO molecules were not included in the refinement while all the rest hydrogen atoms were located by difference maps and refined isotropically. Some of the solvent molecules of crystallization apparently escaped during data collection; three of the Me_2CO molecules have an occupancy factor of 1.0, the fourth has 0.7, and the single *n*-hexane molecule per unit cell—with an occupancy factor of 0.3 and very large temperature factors—is estimated from the very small electron density in the Fourier map and its known presence during the cystallization process. All non-hydrogen atoms, with the exception of those of *n*-hexane, were refined with anisotropic thermal parameters. For **2**·4Me_2CO, all hydrogen atoms [except those of the methyl groups C(54), C(72), C(73), C(82), and C(83) which were introduced at calculated positions as riding on bonded atoms] were located by difference maps and their positions were refined isotropically. The hydrogen atom of the OH^- group was disordered and refined isotropically with occupation factor at 10.5. All non-hydrogen atoms were refined anisotropically. The final values of *R*1 and w*R*2 for **1**·4Me_2CO·0.5C_6H_{14} are 0.0825 and 0.2742 for all data, and 0.0514 and 0.1297 for 7979 reflections with $I > 2\sigma(I)$; for **2**·4Me_2CO they are 0.0469 and 0.0835 for all data and for observed data are listed in Table 1. The maximum and minimum residual peaks in the final difference map were +0.779 and −0.986 e/Å^3 for **1**·4Me_2-CO·0.5C_6H_{14}, and +0.355 and −0.186 e/Å^3 for **2**·4Me_2CO. The largest shift/esd in the final cycle was 0.098 for **1**·4Me_2CO·0.5C_6H_{14} and 0.082 for **2**·4Me_2CO.

Table 1. Crystallographic Data for Complex **2**

parameter	**2**·4Me_2CO
empirical formula	$C_{72}H_{101}Ni_5N_{15}O_{17}$
fw	1742.23
space group	*C*2/*c*
temp, °C	25
λ, Å	0.7107
a, Å	19.085(3)
b, Å	20.142(3)
c, Å	22.574(4)
β, deg	103.30(1)
V, Å^3	8445(2)
Z	4
ρ_{obsd}, g cm^{-3}	1.35(2)
ρ_{calc}, g cm^{-3}	1.370
μ(Mo Kα), mm^{-1}	1.165
*R*1[a]	0.0297
w*R*2[a]	0.0735

[a] $w = 1/[\sigma^2(F_o^2) + (aP)^2 + bP]$ and $P = (\max(F_o^2,0) + 2F_c^2)/3$; $a = 0.0127$, $b = 8.5420$. $R1 = \sum(|F_o| - |F_c|)/\sum(|F_o|)$, $wR2 = \{\sum[w(F_o^2 - F_c^2)^2]/\sum[w(F_o^2)^2]\}^{1/2}$ for 4337 reflections with $I > 2\sigma(I)$.

Results and Discussion

Synthesis. The present work represents one of the first stages[16,21] of a program concerned with developing synthetic methodologies to high-nuclearity M_x (M = Mn, Fe, Co, Ni, Cu; $x \geq 4$) clusters with interesting structural and magnetic

(20) (a) Sheldrick, G. M. *SHELXS-86: Structure Solving Program*; University of Göttingen: Germany, 1986. (b) Sheldrick, G. M. *SHELXL-93: Crystal Structure Refinement*; University of Göttingen: Germany, 1993.

(21) (a) Tangoulis, V.; Paschalidou, S.; Bakalbassis, E.; Perlepes, S. P.; Raptopoulou, C. P.; Terzis, A. *Chem. Commun.* **1996**, 1297. (b) Tangoulis, V.; Raptopoulou, C. P.; Terzis, A.; Paschalidou, S.; Perlepes, S. P.; Bakalbassis, E. G. *Inorg. Chem.* **1997**, *36*, 3996. (c) Tangoulis, V.; Raptopoulou, C. P.; Paschalidou, S.; Bakalbassis, E. G.; Perlepes, S. P.; Terzis, A. *Angew. Chem., Int. Ed. Engl.* **1997**, *36*, 1083. (d) Tangoulis, V.; Raptopoulou, C. P.; Paschalidou, S.; Tsohos, A. E.; Bakalbassis, E. G.; Terzis, A.; Perlepes, S. P.; *Inorg. Chem.* **1997**, *36*, 5270.

properties. One of our strategies takes advantage of the observation that the reactions between metal β-diketonates and benzotriazoles are proven to be a rich source of such products.[16,22,23]

Several groups have been exploring the coordination chemistry of benzotriazoles,[22−24] which is chiefly motivated by the anticorrosion properties of btaH and its ring-substituted derivatives toward certain metals, particularly copper and its alloys.[25] There are only two examples of structurally characterized discrete benzotriazolate complexes containing more than three metal atoms. The first example[24e] is the mixed-valent complex $[Cu_5(bta)_6(t\text{-}C_4H_9NC)_4]$ (**3**) in which an octahedrally coordinated Cu^{II} atom is surrounded by four tetrahedrally coordinated Cu^{I} atoms. This was followed by the report[22a] of the X-ray structure of the remarkable complex $[Cu_5(bta)_6(acac)_4]$ (**4**), which had been isolated before as a powder,[22b] consisting of a distorted tetrahedral arrangement of four five-coordinate Cu^{II} atoms centered on the fifth.

The initial reaction explored was that between $[Ni(acac)_2(H_2O)_2]$ and 1.2 equiv of btaH (5:6) in either CH_2Cl_2 or $MeNO_2$. Both solvents facilitate a rapid reaction, a color change to blue, and the precipitation of sky-blue $Ni_5(bta)_6(acac)_4$ (**1a**), whose formula was established by C, H, N, and Ni analyses. The product is probably oligomeric or polymeric as indicated by the very low solubility in all common organic solvents, including DMF, and its quantitative yield. We initially came across the new compound $[Ni_5(OH)(bta)_5(acac)_4(H_2O)_4]$ (**1**) in relatively low yield (∼15%) from the 5:6 reaction of $[Ni(acac)_2(H_2O)_2]$ with btaH in refluxing Me_2CO. The reaction mixture gave a quantity of product **1a** which was removed by filtration. Layering of the dark blue filtrate with *n*-hexane gave blue crystals; a structural characterization established the formulation $\mathbf{1}\cdot 4Me_2CO\cdot 0.5C_6H_{14}$ for them. A formal balanced equation for the formation of **1** can be written as indicated in eq 1. The

$$5[Ni(acac)_2(H_2O)_2] + 5btaH \rightarrow [Ni_5(OH)(bta)_5(acac)_4(H_2O)_4] + 6acacH + 5H_2O \quad (1)$$

incorporation of OH^- in the product suggests involvement of H_2O from the starting material or/and the solvent. In seeking to increase the yield of **1** and suppress the formation of **1a**, it was logical to increase the water concentration in the reaction mixture. The improved procedure described in the Experimental Section gives higher isolated yields of pure material (70−75%),

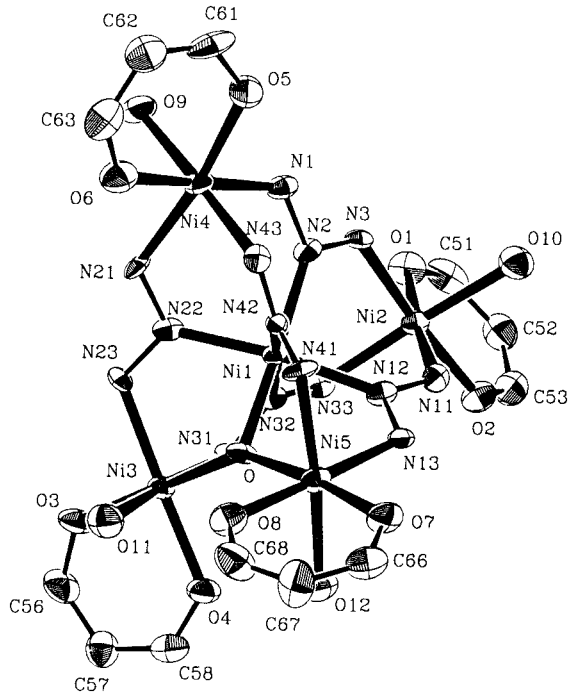

Figure 1. ORTEP view of **1** with 50% thermal ellipsoids showing the atom labeling scheme. To avoid congestion, the methyl groups of $acac^-$ and all bta^- carbon atoms are omitted.

while keeping the yield of **1a** very low (<10%). Further increase of the water concentration to *ca*. 2 M in the reaction mixture prevents all formation of **1a**. This reaction is not particularly sensitive to the btaH/Ni^{II} ratio; ratios from 2:1 to 0.8:1 all gave compound **1** in comparable yields and purity.

Preparation of the analogous 5,6-dimethylbenzotriazolate derivative in a manner similar to that of **1** gave blue-green crystals of $\mathbf{2}\cdot 4Me_2CO$, which analyzed well for the corresponding unsolvated Ni_5 cluster; the insoluble product **2a** appeared in the reaction mixture only in considerably lower H_2O concentrations (<1 M). No doubt this synthetic approach could also be extended to still more ring-substituted benzotriazoles. However, when the corresponding benzoylacetonate and dibenzoylmethanate derivatives were sought, this at-first-glance trivial modification to the reaction led to completely different Ni_9 and Ni_5 clusters, respectively.[23]

Molecular Structures. ORTEP representations of **1** and **2** are shown in Figures 1 and 2, respectively; selected interatomic distances and angles are collected in Tables 2 and 3, respectively.

As has already been reported in our previous communication,[16] the solid-state structure of $\mathbf{1}\cdot 4Me_2CO\cdot 0.5C_6H_{14}$ contains discrete pentameric molecules of formula $[Ni_5(OH)(bta)_5(acac)_4(H_2O)_4]$. The pentameric assembly is composed of a distorted tetrahedral arrangment of four six-coordinate Ni^{II} atoms [Ni(2), Ni(3), Ni(4), Ni(5)] centered on the fifth [Ni(1)]. Each of the five μ_3-bta^- ligands spans an edge of the Ni_4 tetrahedron and is ligated to the central metal, Ni(1), through its central nitrogen atom. The symmetry of the molecule is destroyed due to the presence of the OH^- ion, which bridges Ni(1), Ni(3), and Ni(5) spanning the sixth edge (Ni(3)···Ni(5)) of the tetrahedron. As a result, the interatomic distance Ni(3)···Ni(5) becomes ∼2 Å shorter (3.987(2) Å) than the distances between the other peripheral Ni^{II} atoms which are in the range 5.840(2)−6.072(2) Å. A terminal H_2O molecule and a chelating $acac^-$ ligand complete octahedral coordination at each peripheral metal.

(22) (a) Handley, J.; Collison, D.; Garner, C. D.; Helliwell, M.; Docherty, R.; Lawson, J. R.; Tasker, P. A. *Angew. Chem., Int. Ed. Engl*. **1993**, *32*, 1036. (b) Marshall, J. H. *Inorg. Chem*. **1978**, *17*, 3711.

(23) Tangoulis, V.; Diamantopoulou, E.; Bakalbassis, E.; Raptopoulou, C. P.; Terzis, A.; Perlepes. S. P. Manuscript in preparation.

(24) (a) Skorda, K.; Bakalbassis, E.; Mrozinski, J.; Perlepes, S. P.; Raptopoulou, C. P.; Terzis, A. *J. Chem. Soc., Dalton Trans*. **1995**, 2317 and references therein. (b) Moore, D. S.; Robinson, S. D. *Adv. Inorg. Chem*. **1988**, *32*, 171. (c) Bencini, A.; Gatteschi, D.; Reedijk, J.; Zanchini, C. *Inorg. Chem*. **1985**, *24*, 207. (d) Reedijk, J.; Roelofsen, G.; Siedle, A. R.; Spek, A. L. *Inorg. Chem*. **1979**, *18*, 1947. (e) Himes, V. L.; Mighell, A. D.; Siedle, A. R. *J. Am. Chem. Soc*. **1981**, *103*, 211. (f) Boyd, P. D. W.; Martin, R. L. *J. Chem. Soc., Dalton Trans*. **1981**, 1069. (g) Hendriks, H. M. J.; Birker, P. J. M. W. L.; Verschoor, G. C.; Reedijk, J. *J. Chem. Soc., Dalton Trans.* **1982**, 623. (h) Kokoszka, G. F.; Baranowski, J.; Goldstein, C.; Orsini, J.; Mighell, A. D.; Himes, V. L.; Siedle, A. R. *J. Am. Chem. Soc*. **1983**, *105*, 5627.

(25) (a) Dugdale, I.; Cotton, J. B. *Corros. Sci*. **1963**, *3*, 69. (b) Chadwick, D.; Hashemi, T. *Corros. Sci*. **1978**, *18*, 39. (c) Merk, L. E. *Stud. Conserv*. **1981**, *26*, 73. (d) Schmitt, G. *Br. Corros. J*. **1984**, *19*, 165. (e) Da Costa, S. L. F. A.; Agostinho, S. M. L. *Corrosion (NACE)* **1989**, *45*, 472. (f) Sockalingum, D.; Fleischmann, M.; Musiani, M. M. *Spectrochim. Acta, Part A* **1991**, *47*, 1475 and references therein. (g) Fang, B.-S.; Olson, C. G.; Lynch, D. W. *Surf. Sci*. **1986**, 176, 476 and references therein.

Table 2. Selected Interatomic Distances (Å) and Angles (deg) for Complex **1**·4Me_2CO·0.5C_6H_{14}

		Distances			
Ni(1)···Ni(2)	3.648(2)	Ni(2)···Ni(3)	5.884(2)	Ni(3)···Ni(4)	5.872(2)
Ni(1)···Ni(3)	3.270(2)	Ni(2)···Ni(4)	6.072(2)	Ni(3)···Ni(5)	3.987(2)
Ni(1)···Ni(4)	3.644(2)	Ni(2)···Ni(5)	5.840(2)	Ni(4)···Ni(5)	5.880(2)
Ni(1)···Ni(5)	3.269(2)				
Ni(1)−O	2.044(7)	Ni(2)−N(11)	2.094(9)	Ni(4)−O(9)	2.175(8)
Ni(1)−N(2)	2.065(8)	Ni(2)−N(33)	2.112(8)	Ni(4)−N(1)	2.118(9)
Ni(1)−N(12)	2.066(9)	Ni(3)−O	2.063(7)	Ni(4)−N(21)	2.112(9)
Ni(1)−N(22)	2.047(9)	Ni(3)−O(3)	1.995(8)	Ni(4)−N(43)	2.114(9)
Ni(1)−N(32)	2.065(8)	Ni(3)−O(4)	2.039(8)	Ni(5)−O	2.076(7)
Ni(1)−N(42)	2.065(9)	Ni(3)−O(11)	2.179(8)	Ni(5)−O(7)	1.996(8)
Ni(2)−O(1)	2.024(8)	Ni(3)−N(23)	2.113(9)	Ni(5)−O(8)	2.020(8)
Ni(2)−O(2)	2.018(8)	Ni(3)−N(31)	2.081(9)	Ni(5)−O(12)	2.194(8)
Ni(2)−O(10)	2.194(8)	Ni(4)−O(5)	2.028(8)	Ni(5)−N(13)	2.081(9)
Ni(2)−N(3)	2.063(9)	Ni(4)−O(6)	2.028(9)	Ni(5)−N(41)	2.124(9)
		Angles			
Ni(2)···Ni(1)···Ni(3)	116.4(4)	Ni(2)···Ni(1)···Ni(5)	115.1(5)	Ni(3)···Ni(1)···Ni(5)	75.1(6)
Ni(2)···Ni(1)···Ni(4)	112.8(4)	Ni(3)···Ni(1)···Ni(4)	116.1(4)	Ni(4)···Ni(1)···Ni(5)	116.5(5)
O−Ni(1)−N(2)	177.5(3)	O(10)−Ni(2)−N(3)	88.4(3)	O(9)−Ni(4)−N(43)	177.2(3)
N(12)−Ni(1)−N(22)	172.0(3)	N(11)−Ni(2)−N(33)	91.8(3)	O(5)−Ni(4)−O(6)	89.6(3)
N(32)−Ni(1)−N(42)	172.5(3)	O−Ni(3)−O(3)	174.1(3)	O(9)−Ni(4)−N(1)	88.9(3)
O−Ni(1)−N(22)	84.7(3)	O(4)−Ni(3)−N(23)	175.8(3)	N(21)−Ni(4)−N(43)	94.3(3)
N(2)−Ni(1)−N(32)	93.9(3)	O(11)−Ni(3)−N(31)	171.3(3)	O−Ni(5)−O(7)	173.2(3)
N(12)−Ni(1)−N(42)	92.7(3)	O−Ni(3)−O(4)	90.2(3)	O(8)−Ni(5)−N(13)	175.9(3)
O(1)−Ni(2)−N(11)	174.0(4)	O(3)−Ni(3)−N(31)	98.2(3)	O(12)−Ni(5)−N(41)	169.6(3)
O(2)−Ni(2)−N(3)	174.4(3)	O(11)−Ni(3)−N(23)	91.2(3)	O−Ni(5)−N(13)	90.3(3)
O(10)−Ni(2)−N(33)	175.6(3)	O(5)−Ni(4)−N(21)	170.9(3)	O(7)−Ni(5)−O(12)	89.9(3)
O(1)−Ni(2)−O(2)	88.5(3)	O(6)−Ni(4)−N(1)	178.5(3)	O(8)−Ni(5)−N(41)	93.3(4)
Ni(1)−O−Ni(3)	105.5(3)	Ni(1)−N(22)−N(21)	127.2(7)	Ni(3)−N(31)−N(32)	117.0(6)
Ni(1)−O−Ni(5)	105.0(3)	Ni(1)−N(22)−N(23)	120.0(6)	Ni(4)−N(1)−N(2)	122.1(7)
Ni(3)−O−Ni(5)	148.6(4)	Ni(1)−N(32)−N(31)	118.3(6)	Ni(4)−N(21)−N(22)	120.0(7)
Ni(1)−N(2)−N(1)	125.1(7)	Ni(1)−N(32)−N(33)	127.2(6)	Ni(4)−N(43)−N(42)	119.7(7)
Ni(1)−N(2)−N(3)	123.5(6)	Ni(1)−N(42)−N(41)	119.6(6)	Ni(5)−N(13)−N(12)	114.8(6)
Ni(1)−N(12)−N(11)	126.6(6)	Ni(1)−N(42)−N(43)	126.7(7)	Ni(5)−N(41)−N(42)	115.1(6)
Ni(1)−N(12)−N(13)	120.8(7)	Ni(2)−N(3)−N(2)	124.0(6)		
		Ni(2)−N(11)−N(12)	120.4(6)		
		Ni(2)−N(33)−N(32)	120.3(6)		
		Ni(3)−N(23)−N(22)	115.2(7)		

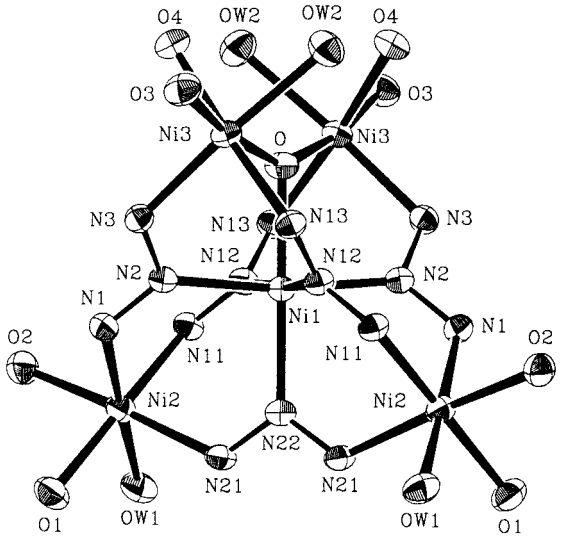

Figure 2. ORTEP view of **2** with 50% thermal ellipsoids showing the atom labeling scheme; for clarity, all carbon atoms are omitted. Identical symbols are used for symmetry-related atoms.

As far as the molecular stucture of **2** is concerned, this is similar to that of **1**. The basic difference is the presence of a 2-fold symmetry axis passing through the central Ni^{II} ion, Ni(1), the hydroxo oxygen atom and N(22) of a bta^- ligand. Consequently, only the half of the molecule is crystallographically independent. As in the case of **1**, the existence of the monatomic hydroxo bridge between Ni(3) and its symmetry-equivalent is responsible for the short Ni(3)···Ni(3) interatomic distance (4.016(1) Å). The rest interatomic distances fall in the same range as for **1**, *i.e.* those corresponding to the edges of the tetrahedron are 5.849(1) and 6.060(1) Å, and those between the central Ni(1) and the apical Ni^{II} atoms are 3.267(1) and 3.633(1) Å (for Ni(1)···Ni(3) and Ni(1)···Ni(2), respectively). Differences in the Ni−O and Ni−N bond lengths between **1** and **2** are not pronounced. The angles subtended at the hydroxo oxygen atom by the three Ni^{II} atoms lie between 104.6(1) and 105.5(3)° for the angles derived from the central metal ion, and they are 148.6(4) and 150.7(2)° for the angle to the peripheral Ni^{II} atoms in **1** and **2**, respectively.

The observed η^3:μ_3 mode of binding for deprotonated benzotriazoles is rare[24b] and was seen previously only in copper[22a,24e,h] and thallium(I)[24d] chemistry. The structures of **1** and **2**, as detailed in the discussion above and in Tables 2 and 3, bear resemblance to that of $[Cu_5(bta)_6(acac)_4]$.[22a] The latter contains five-coordinate peripheral metal ions and an extra bta^- group, instead of μ_3-OH^-, spanning the sixth edge of the Cu_4 tetrahedron. The mixed-valence complex $[Cu_5(bta)_6(t\text{-}C_4H_9NC)_4]$[24e,h] is also somewhat structurally related to compounds **1** and **2**; this involves a central Cu^{II} atom ligated with six nitrogen atoms and four peripheral Cu^{I} atoms, each coordinated to one *tert*-butyl isocyanide ligand and to three different bta^- ligands in an essentially tetrahedral arrangement.

Complexes **1** and **2** join a very small family of discrete Ni^{II} clusters of nuclearity five;[12] as far as we can ascertain, the found

Table 3. Selected Interatomic Distances (Å) and Angles (deg) for Complex **2**·4Me_2CO[a]

		Distances			
Ni(1)···Ni(2)	3.633(1)	Ni(2)···Ni(3)	5.849(1)	Ni(3)···Ni(3)[b]	4.016(1)
Ni(1)···Ni(3)	3.267(1)	Ni(2)···Ni(2)[b]	6.060(1)		
Ni(1)−O	2.053(3)	Ni(2)−O(1)	2.033(2)	Ni(3)−O	2.076(1)
Ni(1)−N(2)	2.064(3)	Ni(2)−O(2)	2.026(2)	Ni(3)−O(3)	2.009(2)
Ni(1)−N(12)	2.040(2)	Ni(2)−OW(1)	2.155(3)	Ni(3)−O(4)	2.042(2)
Ni(1)−N(22)	2.065(3)	Ni(2)−N(1)	2.106(3)	Ni(3)−OW(2)	2.197(3)
		Ni(2)−N(11)	2.103(3)	Ni(3)−N(3)	2.086(3)
		Ni(2)−N(21)	2.088(3)	Ni(3)−N(13)	2.087(3)
		Angles			
Ni(2)···Ni(1)···Ni(2)[b]	113.0(1)	Ni(3)···Ni(1)···Ni(3)[b]	75.9(1)	Ni(2)···Ni(1)···Ni(3)	115.8(1)
Ni(2)···Ni(1)···Ni(3)[b]	115.7(1)				
O−Ni(1)−N(22)	180.0	O(1)−Ni(2)−N(11)	174.0(1)	O−Ni(3)−O(3)	172.1(1)
N(2)−Ni(1)−N(2)[b]	171.6(1)	O(2)−Ni(2)−N(21)	176.3(1)	O(4)−Ni(3)−N(13)	174.9(1)
N(12)−Ni(1)−N(12)[b]	173.2(1)	OW(1)−Ni(2)−N(1)	177.5(1)	OW(2)−Ni(3)−N(3)	170.1(1)
O−Ni(1)−N(2)	85.8(1)	O(1)−Ni(2)−O(2)	88.5(1)	O−Ni(3)−N(3)	87.2(1)
N(2)[b]−Ni(1)−N(12)	92.3(1)	OW(1)−Ni(2)−N(11)	84.3(1)	O(3)−Ni(3)−N(13)	93.3(1)
N(12)[b]−Ni(1)−N(22)	93.4(1)	N(1)−Ni(2)−N(21)	91.7(1)	O(4)−Ni(3)−OW(2)	84.2(1)
Ni(1)−O−Ni(3)	104.6(1)	Ni(1)−N(12)−N(13)	120.3(2)	Ni(2)−N(11)−N(12)	121.1(2)
Ni(3)−O−Ni(3)[b]	150.7(2)	Ni(1)−N(22)−N(21)	124.0(2)	Ni(2)−N(21)−N(22)	123.3(2)
Ni(1)−N(2)−N(1)	127.2(2)	Ni(1)−N(22)−N(21)[b]	124.0(2)	Ni(3)−N(3)−N(2)[b]	115.3(2)
Ni(1)−N(2)−N(3)[b]	120.2(2)	Ni(2)−N(1)−N(2)	119.1(2)	Ni(3)−N(13)−N(12)	114.8(2)
Ni(1)−N(12)−N(11)	126.5(2)				

[a] For atom-labeling scheme, see Figure 2. [b] Symmetry transformation used to generate equivalent atoms: $-x, y, -z + {}^1/_2$.

topological arrangement of five metal ions is unique for nickel(II).

IR and UV/Vis Spectroscopy. In the IR spectra, complexes **1** and **2** exhibit medium sharp bands at 3590 and 3570 cm^{-1}, respectively, assigned to ν(OH) of the μ_3-OH^- group.[11c,26] In addition, they exhibit a broad medium-to-strong $\nu(OH)_{H_2O}$ band at ~3400 and a δ(HOH) shoulder at 1615 cm^{-1}.[26] A series of five strong bands is found in the 1600−1400 cm^{-1} region. Contributions from benzotriazolate ν(C···C) and ν(C···N) vibrations would be expected in this region,[27] but overlap with the $\nu(C\cdots C)_{acac^-}$ and $\nu(C\cdots O)_{acac^-}$ bands[26,28] renders assignments difficult. The bands in the 500−250 cm^{-1} are mainly due to the Ni−O and Ni−N stretching modes.[26,28] The simpler far-IR spectrum of **2** reflects its higher symmetry. As would be expected from the stoichiometry the OH^- and H_2O bands are absent in the spectra of **1a** and **2a**. The IR and far-IR spectra of these complexes are not similar with those of **1** and **2**, respectively, supporting our suggestion that the $acac^-$ ligation mode is different in the former.

The solid-state UV/visible spectra of **1** and **2** are similar exhibiting d−d maxima typical of octahedral Ni^{II}.[29] The bands at λ_{max} values of 615, 635, and 390−357 nm are assigned to the spin-allowed transitions $^3T_{1g} \leftarrow {}^3A_{2g}$ and $^3T_{1g}(P) \leftarrow {}^3A_{2g}$, respectively, under O_h symmetry. The shoulder at ~730 nm definitely originates from the spin forbidden $^1E_g \leftarrow {}^3A_{2g}$ transition frequently observed in octahedral nickel(II) complexes. The appearance of two bands in the region of the $^3T_{1g}(P) \leftarrow {}^3A_{2g}$ transition reflects the different chromophores (NiN_5O, NiN_3O_3, NiN_2O_4) present in **1** and **2**; alternatively, it may suggest a lower symmetry (D_{4h}).[29]

Magnetic Susceptibility Studies. Variable-temperature magnetic susceptibility data performed on powder samples of **1** and **2** between 295 and 5 K are given in the Supporting Information, together with the susceptibilities calculated with the theoretical equation. The room-temperature value of the product $\chi_M T/Ni^{II}$ for **1** (1.02 $cm^3\ mol^{-1}$ K) is what is expected for an $S = 1$ spin value. $\chi_M T$ gradually decreases with the decreasing temperature and reaches (see inset of Figure 3) a value of *ca.* 0.17 $cm^3\ mol^{-1}$ K at 5 K. The room-temperature value of **2** is also 1.02 $cm^3\ mol^{-1}$ K. The $\chi_M T/Ni^{II}$ product gradually decreases with the decreasing temperature but reaches (see Figure 4) a slightly higher value (*ca.* 0.23 $cm^3\ mol^{-1}$ K) than that of **1** at 5 K. Antiferromagnetic interactions are characterized by a regular decrease of $\chi_M T$ as T is lowered. The interaction is most likely intramolecular, because both benzotriazolato and acetylacetonato ligands should afford good intercluster magnetic shielding.

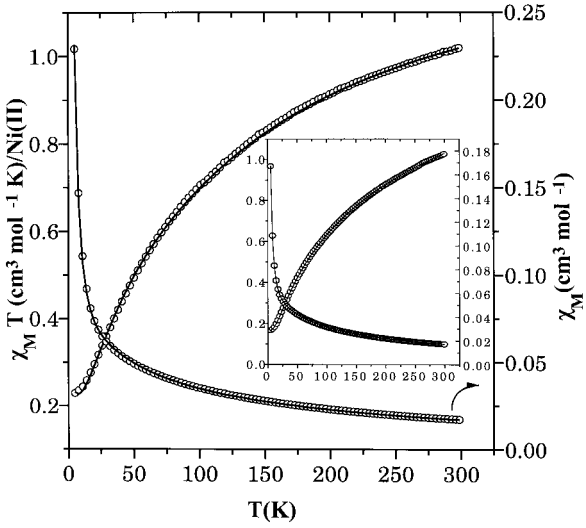

Figure 3. Plots of $\chi_M T/Ni^{II}$ and χ_M/Ni^{II} versus T for a polycrystalline sample of complex $[Ni_5(OH)(5,6diMebta)_5(acac)_4(H_2O)_4]$ (**2**). The solid line represents the fit to the theoretical model; see the text for the fitting parameters. In the inset are shown the corresponding data for complex $[Ni_5(OH)(bta)_5(acac)_4(H_2O)_4]$ (**1**).

The theoretical model to interpret the magnetic susceptibility data for the two clusters was sought. It has to be realized at this point that this is not an easy task, since with five Ni^{II} ($S =$

(26) Nakamoto, K. *Infrared and Raman Spectra of Inorganic and Coordination Compounds*, 4th ed.; Wiley: New York, 1986; pp 227−231, 259−263.
(27) Rubim, J.; Gutz, I. G. R.; Sala, O.; Orville-Thomas, W. J. *J. Mol. Struct.* **1983**, *100*, 571.
(28) Nakamoto, K.; Udovich, C.; Takemoto, J. *J. Am. Chem. Soc.* **1970**, *92*, 3973.
(29) Lever, A. B. P. *Inorganic Electronic Spectroscopy*, 2nd ed.; Elsevier: Amsterdam, 1984; pp 507−520.

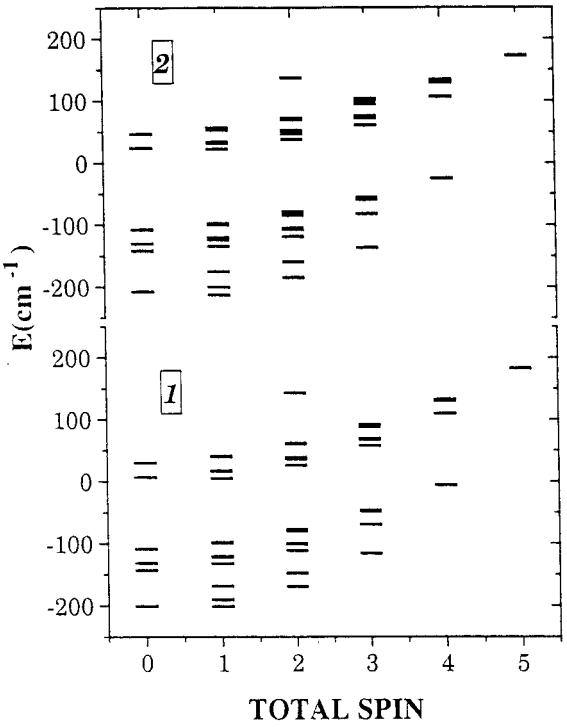

Figure 4. Calculated total spin energy levels for complexes **1** and **2**.

1) ions there is a total degeneracy of $(2S + 1)^5 = 243$. Moreover, due to the low symmetry of **1** and **2**, the Kambe vector-coupling method[30] cannot be used, whereas that of Belorizky,[31] issued for low-symmetry systems, appears rather complicated.

The ground state of nickel(II) in an octahedral environment is orbitally nondegenerate and as such the magnetic exchange interactions between nearest-neighbor metal ions in a cluster are treated with an isotropic spin Hamiltonian

$$H = -2\sum J_{ij} S_i S_j \qquad (2)$$

where J_{ij} is the exchange parameter between the ith and jth paramagnetic ions and S_i and S_j are spin operators on the same ions. The intramolecular magnetic exchange interactions present in the clusters are largely due to interactions between $^3A_2$ Ni^{II} ions as propagated by bridging benzotriazolate anions. It should be stressed at this point that a simplified model (3-J) used to fit the susceptibility data of both **1** and **2**—in which J_1 corresponds to the interaction between the peripheral metal ions, J_2 to the interaction of the central metal with the outer ones, and J_3 stands for the interaction between the peripheral nickels bridged by the μ_3 hydroxo group—led to a very poor fitting with unrealistic values for both the J parameters and the g value. Consequently, there was a need for a different theoretical treatment for both complexes.

Complexes **1** and **2** involve five Ni^{II} ions, four of which are arranged at the apexes of a tetrahedron with the fifth at the center. Moreover, their low symmetry results in unequal distances both between the peripheral metals as well as between the central Ni^{II} ion and the outer ones. Thus, the Hamiltonian should contain (i) a cyclic term, H_{cyc}, of four Ni^{II} ions forming

Scheme 1. Diagram of the Magnetic Exchange Coupling Constants for Complexes **1** and **2** (The Nickel Atom Labeling Scheme Is the Same as that of Figure 1)

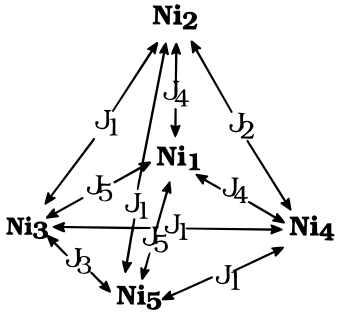

the tetrahedron, (ii) a second term, H_{od}, involving the odd atoms of the pentamer, (iii) a third one, H_{ev}, involving the even atoms and, finally, (iv) a term, H_{cent}, involving the interactions of the central ion, Ni(1), with both the even pair of atoms, $H_{1,ev}$, and the odd pair of atoms, $H_{1,od}$ (Scheme 1), *i.e.*

$$H = H_{cyc} + H_{od} + H_{ev} + H_{cent} (= H_{1,ev} + H_{1,od}) \qquad (3)$$

The explicit form of the spin Hamiltonian in eq 2 has been given in ref 16.

To determine the eigenvalues of the explicit form of the spin Hamiltonian and, subsequently, a close expression of the magnetic susceptibility, the method of hierarchy of algebras,[32] which diagonalizes the isotropic Hamiltonian of nonsymmetrical molecules, was employed. Details of this algebraic part are given in the Appendix.

A theoretical expression for the molar magnetic susceptibility was derived from eq A5 (see Appendix) by means of the Van Vleck equation. This leads to

$$\chi_M = \frac{N\beta^2 g^2}{3kT} \frac{\sum_{i=1}^{51} a_i \exp(-E_i/kT)}{\sum_{i=1}^{51} b_i \exp(-E_i/kT)} + N\alpha \qquad (4)$$

The summations in eq 4 run over all spin states of the complex, where each energy state is characterized by a total spin S_T and energy E_i, $N\alpha$, is the temperature-independent paramagnetism of the complex, and the other symbols have their usual meaning. Moreover, the values of a_i [$= S_T(S_T + 1)(2S_T + 1)$] and b_i [$= (2S_T + 1)$] are given in Table 4.

The analytical eq A5 (see Appendix) of the spin Hamiltonian was used to explain the magnetic exchange interactions of the pentanuclear Ni^{II} clusters. The excellent fit derived further verifies our choice to ignore the last part of the Hamiltonian, which makes a negligible contribution compared to its other parts. This was further substantiated through the evaluation of the eigenvalues of the Hamiltonian, affording very small coefficients for this last term in comparison to those of the others. By assuming (i) a very small and negative D value,[24f] (ii) the same spectroscopic splitting constant, g, for all the individual Ni^{II} atoms, (iii) negligible intercluster exchange interactions,[33] and by fixing $N\alpha$[11e] at 400×10^{-6} cm^3 mol^{-1}, an excellent fit (the fitting procedure is described in ref 16) of the experimental data of complex **1** was obtained from the

(30) (a) Kambe, K. *J. Phys. Soc. Jpn*. **1950**, *5*, 48. (b) Hatfield, W. E. In *Theory and Applications of Molecular Paramagnetism*; Bourdeaux, E. A., Mulay, L. N., Eds.; Wiley-Interscience: New York, 1976; Chapter 7.
(31) Belorizky, E.; Fries, P. H. *J. Chim. Phys.* **1993**, *90*, 1077 and references therein.
(32) Theophilou, A. K.; Thanos, S. *Physica B* **1994**, *202*, 41, 47.
(33) Ginsberg, A. P.; Martin, R. L.; Brookes, R. W.; Sherwood, R. C. *Inorg. Chem*. **1972**, *11*, 2884.

Table 4. Parameters of the Susceptibility Equation

	S_{24}	S_{35}	S_T	b_i	a_i		S_{24}	S_{35}	S_T	b_i	a_i
E_1	2	2	5	11	330	E_{27}	1	2	3	7	84
E_2	2	2	4	9	180	E_{28}	1	2	2	5	30
E_3	2	2	3	7	84	E_{29}	1	2	3	7	84
E_4	2	2	4	9	180	E_{30}	1	2	2	5	30
E_5	2	2	3	7	84	E_{31}	1	2	1	3	6
E_6	2	2	2	5	30	E_{32}	1	2	2	5	30
E_7	2	2	3	7	84	E_{33}	1	2	1	3	6
E_8	2	2	2	5	30	E_{34}	1	2	0	1	0
E_9	2	2	1	3	6	E_{35}	1	1	3	7	84
E_{10}	2	2	2	5	30	E_{36}	1	1	2	5	30
E_{11}	2	2	1	3	6	E_{37}	1	1	1	3	6
E_{12}	2	2	0	1	0	E_{38}	1	1	2	5	30
E_{13}	2	2	1	3	6	E_{39}	1	1	1	3	6
E_{14}	2	1	4	9	180	E_{40}	1	1	0	1	0
E_{15}	2	1	3	7	84	E_{41}	1	1	1	3	6
E_{16}	2	1	2	5	30	E_{42}	1	0	2	5	30
E_{17}	2	1	3	7	84	E_{43}	1	0	1	3	6
E_{18}	2	1	2	5	30	E_{44}	1	0	0	1	0
E_{19}	2	1	1	3	6	E_{45}	0	2	3	7	84
E_{20}	2	1	2	5	30	E_{46}	0	2	2	5	30
E_{21}	2	1	1	3	6	E_{47}	0	2	1	3	6
E_{22}	2	1	0	1	0	E_{48}	0	1	2	5	30
E_{23}	2	0	3	7	84	E_{49}	0	1	1	3	6
E_{24}	2	0	2	5	30	E_{50}	0	1	0	1	0
E_{25}	2	0	1	3	6	E_{51}	0	0	1	3	6
E_{26}	1	2	4	9	180						

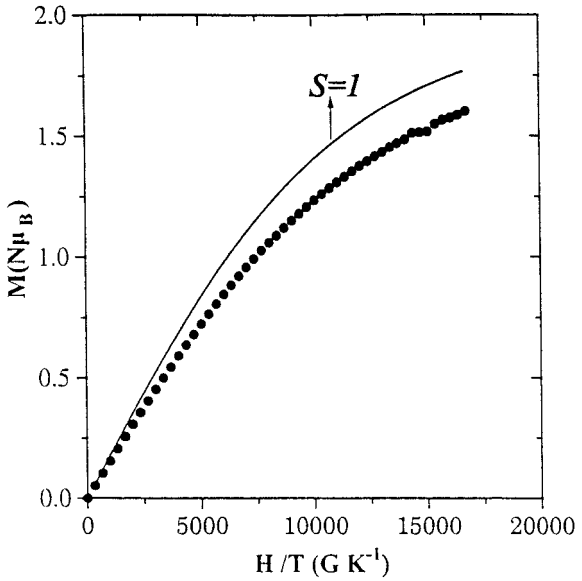

Figure 5. Magnetization study of **1** at 3 K over the field range 0−5 T. The solid line represents the theoretical curve for the $S = 1$ state.

following set of parameters: $J_1 = -5.0$ cm^{-1}, $J_2 = -10.7$ cm^{-1}, $J_3 = -39.6$ cm^{-1}, $J_4 = -6.1$ cm^{-1}, $J_5 = -4.4$ cm^{-1}, $g = 2.2$-(1) (solid line in inset of Figure 3) with a reliability factor of $R = 0.17 \times 10^{-6}$ [$R = \sum_n(\chi_{exptl} - \chi_{calcd})^2$].

The energies of the spin levels obtained with the above values are given in Figure 4. It is obvious that the ground state of **1** is a singlet with an energy difference from the first excited state ($S = 1$) of only 0.3 cm^{-1}. In particular, the energy scheme obtained by this set of parameters clearly shows that the ground state of complex **1** is a mixture of a singlet $S = 0$ and a triplet $S = 1$ state since these two states are separated by only 0.3 cm^{-1}. In an attempt to verify further the nature of the ground state of **1**, the field dependence of its magnetization was also recorded at 3 K (Figure 5). The solid line in this figure is the theoretical Brillouin function for $S = 1$. The non-Brillouin behavior of the magnetization data of **1** is mostly in line with

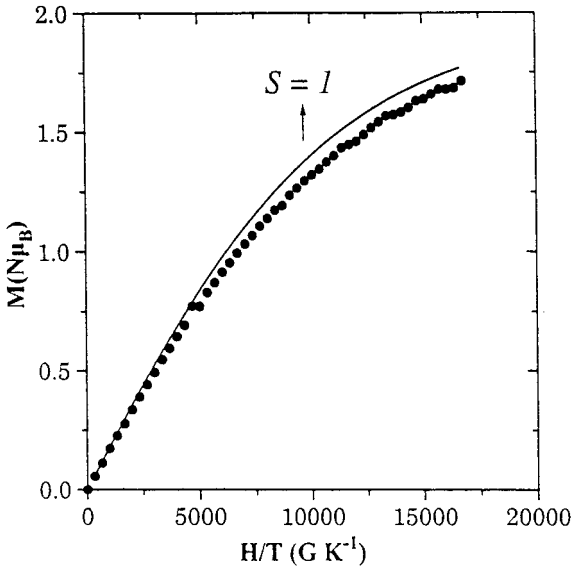

Figure 6. Magnetization study of **2** at 3 K over the field range 0−5 T. The solid line represents the theoretical curve for the $S = 1$ state.

an admixture of the two states. An intermediate-spin ground state has also been observed in other high-nuclearity clusters.[21d,34]

Following an analogous to **1** procedure for the magnetic susceptibility study of complex **2**, the five-J model gives for the latter very similar exchange parameters to those of **1**, *i.e.*: $J_1 = -3.9$ cm^{-1}, $J_2 = -10.4$ cm^{-1}, $J_3 = -43.2$ cm^{-1}, $J_4 = -5.9$ cm^{-1}, $J_5 = -3.1$ cm^{-1}, $g = 2.2(1)$ (solid line of Figure 3), where $R = 0.17 \times 10^{-6}$. The corresponding energies of the spin levels, shown also in Figure 4, clearly shows that the ground state is a triplet with an energy difference from the first excited state ($S = 0$) of *ca.* 4.9 cm^{-1}. This is further substantiated by the field dependence of the magnetization recorded at 3 K, shown in Figure 6, which shows that the triplet ground state is more sufficiently populated, due to the fact that the magnetization data of **2** are closer to the theoretical Brillouin function for the $S = 1$ state. *Consequently, there seems to be a relationship between the symmetry of the cluster and its ground-state spin value; the latter increases as the former increases.*

The negative J parameters imply intracluster antiferromagnetic interactions for both pentanuclear clusters. Therefore, the exchange network for **1** and **2** is formed by five antiferromagnetic-type exchange interactions as a consequence of their low symmetry.

The presence of a state with an integer spin which is thermally populated at 4.2 K is confirmed by the EPR spectra of both **1** and **2**; they show a transition at *ca.* 1000 G due to zero-field splitting effects.[13a] The fact that the low-field transitions are more intense than the high-field ones is in line with a negative and small D value.[34b] All these are in excellent agreement with the assumption made for the D value in the fitting procedure.

Quantum-Chemical Interpretation of the Exchange Mechanism. The low symmetry of the clusters makes difficult a thorough study of the exchange interaction mechanism in **1** and **2**; however, a qualitative interpretation of the mechanism could be proposed. Ginsberg[35] and Anderson,[36] dealing with the

(34) (a) Barra, A.-L.; Gatteschi, D.; Pardi, L.; Müller, A.; Döring, J. *J. Am. Chem. Soc.* **1992**, *114*, 8509. (b) Delfs, C.; Gatteschi, D.; Pardi, L.; Sessoli, R.; Wieghardt, K.; Hanke, D. *Inorg. Chem.* **1993**, *32*, 3099.
(35) Ginsberg, A. P. *Inorg. Chim. Acta* **1971**, *5*, 45.
(36) Anderson, P. W. In *Magnetism*; Rado, G. T., Suhl, H., Eds.; Academic Press: New York, 1963; Vol. 1.

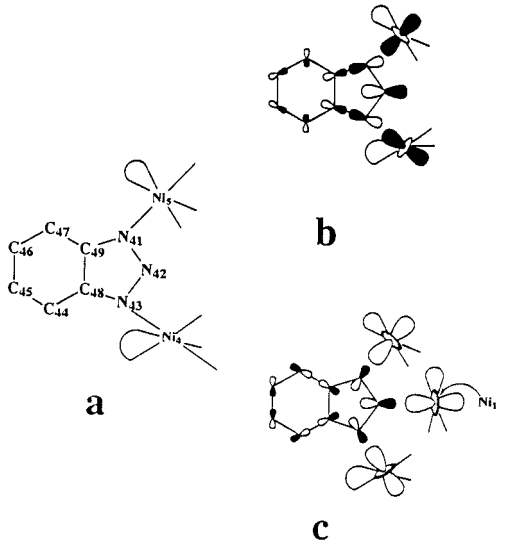

Figure 7. Hypothetical benzotriazolate-bridged Ni(4)···Ni(5) dimer in **1** (a), along with its Ni(5)−N(41)−C(49)−C(48)−N(43)−Ni(4) (b), and Ni(5)−N(41)−N(42)−N(43)−Ni(4), Ni(4)−N(43)−N(42)−Ni(1), and Ni(5)−N(41)−N(42)−Ni(1) exchange pathways (c).

interpretation of exchange interactions, have stressed the application of qualitative symmetry arguments to predict and explain the sign and magnitude of the exchange integral, *J*. It is recognized that when two metal ions are chemically bonded to a common set of closed shell atoms—the unit comprising a bridged dinuclear system—any unpaired electrons originating from d orbitals on the metals will delocalize through extended molecular orbitals onto the bridge. The nature of the interaction between the unpaired electrons associated with the two metal centers is governed by the symmetry between the atomic orbitals in which these electrons reside. Moreover, Ginsberg and coworkers[11g] have shown that, in the case of the cubane-type Ni^{II} tetramers consisting of four Ni^{II} and four oxygen atoms from four bridging methoxide groups, the contribution by each Ni−O−Ni pathway will be determined by (i) the magnitude of the relevant overlap integrals, (ii) the Ni−O distance, (iii) the Ni−O−Ni angle, and (iv) the relative energies of the nickel(II) and oxygen orbitals. However, if the Ni^{II} ions are not linked by monatomic bridges but the connecting orbitals are multicenter molecular orbitals, the coupling can take place over long distances and through polyatomic bridges.[33] This is the case with both **1** and **2** for which our magnetic measurements strongly support the fact that the spins of the five metal ions interact antiferromagnetically. However, the sign and the magnitude of the magnetic exchange in superexchange-coupled systems are determined by the overlap between the magnetic orbitals, their energy gap, and their two-electron exchange integral.[24f,37] Consequently, the antiferromagnetic exchange interactions observed in **1** and **2** could be explicable on simple symmetry considerations as well as with the aid of quantum-chemical calculations.

The magnetic exchange interactions of **1** are examined first. It is assumed that **1** consists of several hypothetical benzotriazolate-bridged $Ni^{II}\cdots Ni^{II}$ dimers. The Ni(4)···Ni(5) dimer is shown in Figure 7 (C_{2v} is the symmetry group of the dimer). As shown in the figure, the benzotriazolate bridge is symmetric in its interaction with the two nickel ions. However, if the unpaired electrons of Ni(4) are delocalized into a certain bridge molecular orbital, because of the symmetry of this bridge the

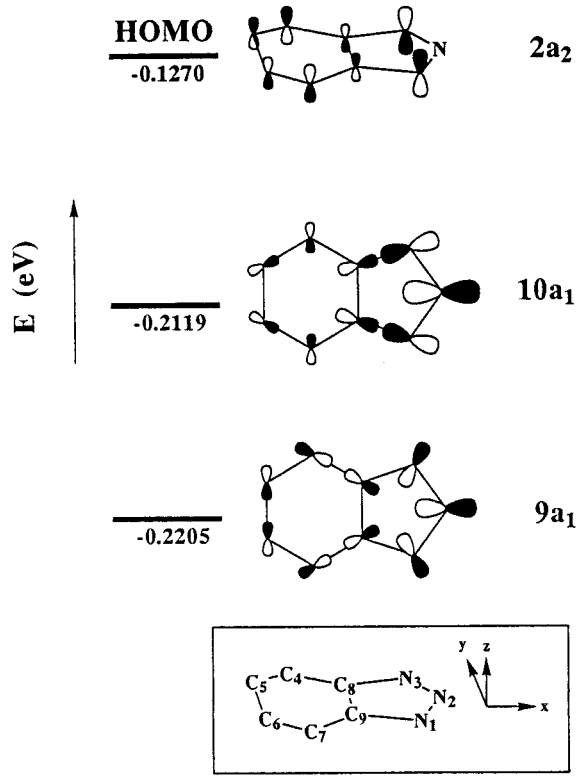

Figure 8. HOMO, $2a_2$, and the $9a_1$ and $10a_1$ MOs derived by CNDO calculations on the bridging benzotriazolate anion.

unpaired electrons on Ni(5) will also be delocalized into the same bridge molecular orbital. Thus, in the case of the hypothetical Ni(4)···Ni(5) dimer, there is an antiferromagnetic mechanism operative. The e_g (O_h designation) orbitals on the Ni^{II} ions span the a_1 representation in the C_{2v} point group. CNDO calculations were completed on the bridging benzotriazolate anion and it was found that in the five highest energy filled orbitals there are two a_1 symmetry orbitals, $9a_1$ and $10a_1$ MOs, these being only about 0.1 eV lower in energy than the HOMO (Figure 8). Both a_1 MOs are σ-type mostly "lone pair" on the N(1), N(2), and N(3) atoms. In particular, $9a_1$ is an in-phase $p_{x,y-\text{hybrid}}$ N(3)−p_x N(2)−$p_{x,y-\text{hybrid}}$ N(1) σ combination and $10a_1$ an in phase $p_{x,y-\text{hybrid}}$ N(3)−$p_{x,y-\text{hybrid}}$ (C8)−$p_{x,y-\text{hybrid}}$ (C9)−$p_{x,y-\text{hybrid}}$ (N1) one. Bonding propagated through these two bridge orbitals leads to the observed antiferromagnetic interaction with a $J_{Ni(5)\cdots Ni(4)}$ value of -5.0 cm^{-1}. Moreover, due to their nature (Figure 7b), $10a_1$ favors N(43)−N(41) magnetic exchange interactions (see also Figure 1 and Chart 1) through its in-phase σ-type N(43)−C(48)−C(49)−N(41) orbital pathway, whereas $9a_1$ favors both N(43)−N(41) and N(43)−N(42) or N(42)−N(41) magnetic exchange interactions through its in-phase N(43)−N(42)−N(41) orbital pathway (Figure 7c). However, owing to the low symmetry of the cluster, the orientation of $e_g(d_{z^2})$ and $9a_1$ orbitals in this case does not favor a strong overlap. As a matter of fact, both Ni(4) and Ni(5) are well below (Table 5) the azolate ring mean plane involving the N(43), N(42), and N(41) atoms by 0.371(2) and 0.276(2) Å, respectively. This, along with the long Ni···Ni distance and the triply bridging function of the benzotriazolate anion, could well account for the low $J_{Ni(5)\cdots Ni(4)}$ value. Furthermore, this should be also the case with the Ni(3)···Ni(4), Ni(3)···Ni(2), and Ni(2)···Ni(5) interactions, since in these pairs the Ni^{II} ions are bridged in a quite analogous way to that of Ni(4)···Ni(5) (Chart 1 and Table 5); hence, their *J* values should be expected equal in close agreement with our assumptions made for the

(37) (a) Mackey, D. J.; Martin, R. L. *J. Chem. Soc., Dalton Trans*. **1978**, 702. (b) Kahn, O. *Inorg. Chim. Acta* **1982**, *62*, 3.

Chart 1. Bridging Function of Each bta− in the Ni(4)···Ni(5), Ni(5)···Ni(2), Ni(2)···Ni(3), and Ni(3)···Ni(4) Pairs of **1** (For Clarity Only the Nitrogen Atoms of Each bta− Are Shown)

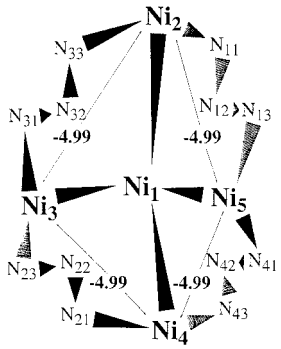

Table 5. Deviations of the Ni^{II} Atoms of **1** and **2** from the Azolate Ring Mean Planes

azolate ring mean plane, consisting of atoms	Ni^{II} ion	deviation (Å)[a,b]
N(1), N(2), N(3), C(8), C(9)	Ni(1) [Ni(1)[c]]	0.108(2) [0.007(2)]
	Ni(2) [Ni(2)[c]]	0.113(2) [0.495(2)]
	Ni(4) [Ni(3)[c]]	−0.109(2) [0.158(2)]
N(11), N(12), N(13), C(18), C(19)	Ni(1) [Ni(1)[c]]	0.030(2) [0.052(2)]
	Ni(2) [Ni(2)[c]]	−0.325(2) [0.288(2)]
	Ni(5) [Ni(3)[c]]	−0.327(2) [0.475(2)]
N(21), N(22), N(23) [N(21)[c]], C(28), C(29) [C(28)[c]]	Ni(1) [Ni(1)[c]]	−0.025(2) [0.000(2)]
	Ni(3) [Ni(2)[c]]	−0.431(2) [0.103(2)]
	Ni(4) [Ni(2)[c]]	−0.333(2) [−0.103(2)]
N(31), N(32), N(33), C(38), C(39)	Ni(1)	−0.265(2)
	Ni(2)	−0.549(2)
	Ni(3)	−0.224(2)
N(41), N(42), N(43), C(48), C(49)	Ni(1)	0.125(2)
	Ni(4)	−0.371(2)
	Ni(5)	−0.276(2)

[a] A negative value implies that the metal ion is below the mean plane, whereas a positive value implies a Ni^{II} atom above the plane. [b] Values in brackets correspond to complex **2**. [c] This atomic labeling scheme refers to complex **2**; see Figure 2.

construction of the Hamiltonian of the system. The magnetic properties of a structurally characterized 1,3-bridging benzotriazolate Cu^{II} complex have been examined.[24g] It exhibits a higher J value of -18 cm^{-1} than that derived for the $J_{Ni(5)\cdots Ni(4)}$ and the similar peripheral interactions of **1**. The doubly bridging (η^1:η^1:μ_2) function of bta$^-$ in the Cu^{II} complex could well account for its larger J value.

Surprisingly, the exchange parameter value of both Ni(1)···Ni(5) and Ni(1)···Ni(3) interactions ($J_5 = -4.4$ cm^{-1}) was derived almost equal to those of the Ni(5)···Ni(4), Ni(3)···Ni(4), Ni(3)···Ni(2), and Ni(2)···Ni(5) ones ($J_1 = -5.0$ cm^{-1}). Contrary to the latter interactions, the metal magnetic centers in the Ni(1)···Ni(3) and Ni(1)···Ni(5) interactions are bridged in a similar way through the three bridging ligands shown in Chart 2. For example, the three bridges for the Ni(1)···Ni(5) pair are the two N(42)−N(41) and N(12)−N(13) diatomics of two different bta$^-$, and the triply bridging (μ_3) oxygen atom of the hydroxo bridge. The two bridging diatomics N(42)−N(41) and N(12)−N(13) could propagate the exchange interactions through the $9a_1$ MO's orbital pathway of bta$^-$. Moreover, O could propagate additional antiferromagnetic interactions as both Ni(1)−O−Ni(5) and Ni(1)−O−Ni(3) angles (*ca.* 105°) are well above the limit (*ca.* 100°) from which the Ni−μ_3(OH)$^-$−Ni interactions become antiferromagnetic.[10,11a,c,e,13a,38] Possibly, the slightly smaller J values derived for the Ni(1)···Ni(5) and Ni(1)···Ni(3) interactions, as compared to J_1, could be the result

Chart 2. Bridging Function in the Ni(1)···Ni(3) and Ni(1)···Ni(5) Pairs of **1** (For Clarity Only the Nitrogen Atoms of Each bta− Are Shown)

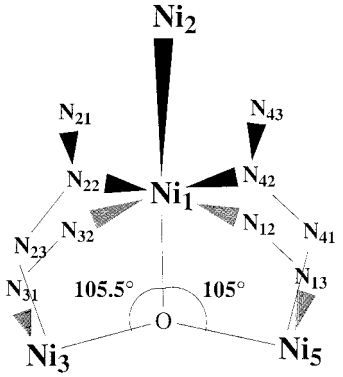

Chart 3. Bridging Function in the Ni(1)···Ni(2) and Ni(1)···Ni(4) Pairs of **1** (For Clarity Only the Nitrogen Atoms of Each bta− Are Shown)

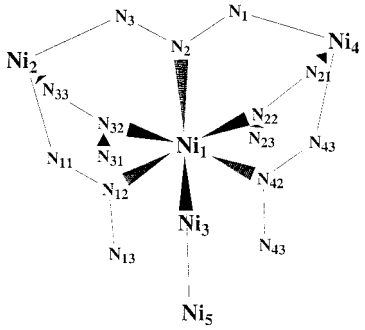

of a decrease of the electron density on the bridging atoms,[39] due to (i) the triply bridging function of both OH$^-$ and bta$^-$, and (ii) unfavorable orbital orientation (low symmetry) leading to a less favorable e_g-9a_1 orbital interaction. As a matter of fact, the overlaps between the metals and the nitrogen atoms are partially compensated by the fact that the former are below or above the mean planes of the azolate rings. For example, regarding the Ni(1)···Ni(3) interaction, both Ni(1) and Ni(3) are below the azolate ring mean plane involving atoms N(31), N(32), and N(33) by *ca.* 0.27 and 0.22 Å, respectively; see Table 5. This is also the case with the relative positions betwen the rest azolate rings and the Ni^{II} atoms involved in the Ni(1)···Ni(5) and Ni(1)···Ni(3) interactions. Again the similarity between the superexchange pathways in the Ni(1)···Ni(3) and Ni(1)···Ni(5) interactions could well account for their equal J values in agreement with the assumptions made for the construction of the Hamiltonian of the system.

The higher J_4 value (-6.1 cm^{-1}) derived for both Ni(1)···Ni(2) and Ni(1)···Ni(4) interactions, as compared to J_5, is examined next. Not unlike the latter, the former possesses three bridges (Chart 3), these being the N(32)−N(33), N(12)−N(11), and N(2)−N(3) diatomics of three different bta$^-$ ligands for the Ni(1)···Ni(2) interactions, and the N(22)−N(21), N(42)−N(43), and N(2)−N(1) diatomics for the Ni(1)···Ni(4) ones. However, as it was shown before, the contribution of the N(32)−N(33) and N(12)−N(11) ligand parts in the magnitude of the overlaps between the metals and the nitrogen atoms is not that favorable. On the contrary, the contribution of the N(2)−N(3)

(38) Brechin, E. K.; Gould, R. O.; Harris, S. G.; Parsons, S.; Winpenny, R. E. P. *J. Am. Chem. Soc.* **1996**, *118*, 11293.
(39) Hay, P. J.; Thibeault, J. C.; Hoffmann, R. *J. Am. Chem. Soc.* **1975**, *97*, 4884.

Chart 4. Ni(3)−O−Ni(5) Angle in Complex **1**

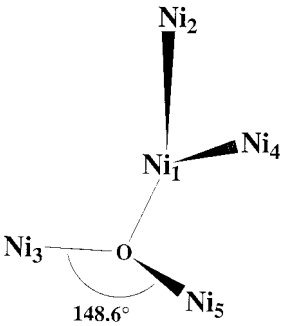

Chart 5. "Symmetric" Ni(4)−N(1)−N(2) and Ni(2)−N(3)−N(2) Angles in **1**, along with the Less "Symmetric" Ni(2)−N(11)−N(12) and Ni(5)−N(13)−N(12) Ones (For Clarity Only the Nitrogen Atoms of Each bta− Are Shown)

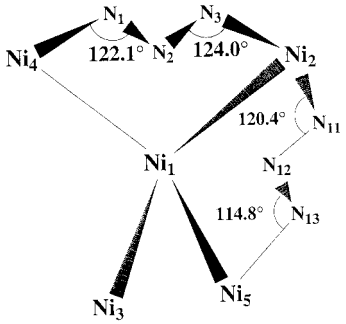

and N(2)−N(1) parts in the magnitude of the corresponding antibonding overlaps is more favorable (*vide infra*), due to the better coplanarity between the Ni(1), Ni(2), and Ni(4) ions and the N(3)−N(2)−N(1) azolate moiety. This in turn, could further increase the magnitude of the relevant overlap integrals. Due to their analogous exchange pathways, the *J* values of the Ni(1)···Ni(2) and Ni(1)···Ni(4) interactions should be expected equal. The magnetic properties of the structurally characterized complex $[Ni_3(1,2\text{-}\mu_2\text{-bta})_6L_6]\cdot 2PPh_3O$ (L = allylamine) have been studied.[24f] It exhibits a higher *J* value (-10.1 cm^{-1}) between adjacent Ni^{II} atoms than that derived for both Ni(1)···Ni(5)/Ni(1)···Ni(3)- and Ni(1)···Ni(2)/Ni(1)···Ni(4)-type interactions. The doubly bridging mode of bta$^-$ (η^1:η^1:μ_2) in the trinuclear Ni^{II} compound could well account for its higher *J* value.

The large Ni(3)−O−Ni(5) angle (148.6°), see Chart 4, along with the considerably short peripheral Ni(3)···Ni(5) distance [3.987(2) Å], could well account[10,11a,c,f,13a,38] for the highest J_3 value of -39.6 cm^{-1} of **1** derived for the Ni(3)···Ni(5) interaction.

Finally, it has been found that the $J_{Ni(2)\cdots Ni(4)}$ value of -10.7 cm^{-1} (J_2) is the second highest one in **1**. The only bridging unit between the two Ni^{II} magnetic centers is that of N(1)−N(2)−N(3). The situation appears quite analogous to that, for example, of the Ni(2)···Ni(5) interaction (J_1). However, this latter exhibits a *J* value (-5.0 cm^{-1}) only half that between Ni(2) and Ni(4). Despite the similarities in their polyatomic bridging units, one should observe that both the Ni(4)−N(1)−N(2) and Ni(2)−N(3)−N(2) angles [122.1(7) and 124.0(6)°, respectively; see Chart 5] are larger and more "symmetric" than those of the Ni(2)···Ni(5) interaction [120.4(6), 114.8(6)°], hence leading to a better overlapping with the e_g metal orbitals. This is further substantiated by (i) the nature of the highest a_1 MOs of the bta$^-$ anion, these being mostly in-phase $p_{x,y-hybrid}$ σ-combinations of their N(1) and N(3) atoms, and (ii) the fact that both Ni(2) and Ni(4) deviate from the corresponding azolate ring mean plane by no more than 0.12 Å; see Table 5. Consequently, the overlap between the e_g metal orbitals and the $9a_1$ and/or $10a_1$ MOs should be larger in this case, affording an increased $J_{Ni(2)\cdots Ni(4)}$ value in fair agreement with the results of our fitting and our assumptions set forth for the construction of the Hamiltonian of the system.

As far as the *J* values derived for **2** are concerned, the following arguments could be made. The larger Ni(3)−O−Ni(5) angle of 150.7° in **2**, *i.e.* the angle Ni(3)−O−Ni(3) in Figure 2, as compared to that of **1** (148.6°), could well account for its higher $J_{Ni(3)\cdots Ni(5)}$ value of -43.2 cm^{-1} (J_3). Additionally, this is one of the highest antiferromagnetic *J* values ever derived[15a,40] for dinuclear and polynuclear Ni^{II} complexes. The similarity of the Ni−N−N angles and the other structural characteristics of the azolate bridges of Ni(4) [Ni(2*) in **2**] and Ni(2) between **1** and **2** explains well the close proximity observed between their *J* values (-10.7 cm^{-1} in **1**, -10.4 cm^{-1} in **2**). Moreover, through an analogous justification, the close proximity in the J_4 value (-6.1 cm^{-1} in **1**, -5.9 cm^{-1} in **2**) could well be understood. However, the smaller Ni(1)−O−Ni(3) angle of **2** [104.6(1)° versus 105.5(3)° in **1**] could give rise to a weaker antiferromagnetic exchange interaction (J_5) between Ni(1) and Ni(3); the derived values are -4.4 cm^{-1} for **1** and -3.1 cm^{-1} for **2**. Finally, the smaller J_1 value of -3.9 cm^{-1} in **2** (-5.0 cm^{-1} in **1**) could be due to less favorable Ni^{II}−azolate orbital interactions, since the appropriate Ni^{II} atoms of **2** deviate more from the bridging azolate ring mean planes (Table 5).

Conclusion

Our goal when beginning this work was to isolate new superparamagnetic clusters, but we have not been successful so far. Nevertheless, we managed to prepare the remarkable pentanuclear Ni^{II} clusters $[Ni_5(OH)(Rbta)_5(acac)_4(H_2O)_4]$ (RbtaH = benzotriazole and 5,6-dimethylbenzotriazole) and described their structures and magnetic properties. The complexes have a novel structure in the solid state. Moreover, a detailed theoretical magnetic model has been derived for both clusters by using the method of hierarchy of algebras to interpret the variable-temperature magnetic susceptibility data. A very good least-squares fit of the data to the theoretical equation was obtained with reasonable magnetic exchange parameters. These results, along with the isothermals of magnetization as a function of *H*/*T*, clearly show that both complexes exhibit an intermediate ground state (a singlet and a triplet). It seems that the spin value of the ground state increases when the symmetry of the cluster increases. This latter conclusion is based on both the present results and the magnetic study of the totally symmetric pentanuclear cluster $[Ni_5(5Mebta)_6(dbm)_4(Me_2CO)_4]$ (dbmH = dibenzoylmethane; 5MebtaH = 5-methylbenzotriazole), which reveals[23] an intermediate spin [$S = 1$, $S = 2$] ground state. CNDO calculations performed on the intervening bta$^-$ bridges have shown that the theoretical *J* parameter trend is in close agreement to that obtained experimentally. Accordingly, the most suitable orbital pathways—all of σ-type—propagating the

(40) (a) Beissel, T.; Birkelbach, F.; Bill, E.; Glaser, T.; Kesting, F.; Krebs, C.; Weyhermüller, T.; Wieghardt, K.; Butzlaff, C.; Trautwein, A. X. *J. Am. Chem. Soc*. **1996**, *118*, 12376. (b) McLachlan, G. A.; Fallon, G. D.; Martin, R. L.; Moubaraki, B.; Murray, K. S.; Spiccia, L. *Inorg. Chem*. **1994**, *33*, 4663. (c) Nanda, K. K.; Das, R.; Thompson, L. K.; Venkatsubramanian, K.; Paul, P.; Nag, K. *Inorg. Chem*. **1994**, *33*, 1188. (d) Chaudhuri, P.; Weyhermüller, T.; Bill, E.; Wieghardt, K. *Inorg. Chim. Acta* **1996**, *252*, 195.

magnetic exchange interaction were verified. Finally, from a synthetic inorganic viewpoint, the preparation of **1** and **2** shows that the transition metal/benzotriazolate/β-diketonate chemistry continues[22a,24e] to be a source of unusual polynuclear metal assemblies.

Acknowledgment. This work was supported by the Greek General Secretariat of Research and Technology (PLATON Program 1583 to E.B. and Grant 91ED to S.P.P.), the Greek Secretariat of Athletics, OPAP (to A.T.), and Mrs. Athina Athanassiou (V.T.).

Appendix. Details of the Algebraic Part of the Hierarchy of Algebras Method

The development of the hierarchy of algebras method yields Casimir operators[41] which diagonalize the largest part of the Hamiltonian directly. The rest of it could be either left for perturbation treatment or treated explicitly through an exact calculation of the nonzero off-diagonal matrix elements.

According to the method of hierarchy of algebras, the following operators should be defined first:

$$b_{24} = S_2 + S_4$$

$$b_{35} = S_3 + S_5$$

$$b_0 = b_{24} + b_{35}$$

$$b_1 = b_{35} - b_{24}$$

Next, by using these operators, a subalgebra A_1 is formed, the Casimir operators of which are

$$C_1 = b_0 b_0 + b_1 b_1$$

$$b_0 b_1 = {b_{24}}^2 - {b_{35}}^2$$

Consequently, the first cyclic part, H_{cyc}, of the Hamiltonian in eq 3, after the expression of the spin products by the defined operators, becomes

$$H_{cyc} = -J_1({b_0}^2 - C_1/2) \qquad \text{(A1)}$$

its two next terms,

$$H_{od} = S_3 S_5 = C_1/8 + (b_0 b_1)/4 - 2 \qquad \text{(A2)}$$

$$H_{ev} = S_2 S_4 = C_1/8 - (b_0 b_1)/4 - 2 \qquad \text{(A3)}$$

and its last part, H_{cent}.

$$H_{cent} = (J_4 + J_5)(S_1 b_0) + (J_4 - J_5)(S_1 b_1) \qquad \text{(A4)}$$

(41) Elliot, J. P.; Dawber, P. G. *Symmetry in Physics*; MacMillan: London, 1990; Vol. 1.

Table A1. The Evaluation of the Casimir Operators According to the Method of Hierarchy of Algebras[a]

S_{24}	S_{35}	$S_{24}+S_{35}$	S_T	${b_{24}}^2$	${b_{35}}^2$	C_1	${b_0}^2$	$b_0 b_1$	$(S_1+b_0)^2$
		4	5, 4, 3				20		30, 20, 12
		3	4, 3, 2				12		20, 12, 6
2	2	2	3, 2, 1	6	6	24	6	0	12, 6, 2
		1	2, 1, 0				2		6, 2, 0
		0	1				0		2
		3	4, 3, 2				12		20, 12, 6
2	1	2	3, 2, 1	6	2	16	6	−4	12, 6, 2
		1	2, 1, 0				2		6, 2, 0
2	0	2	3, 2, 1	6	0	12	6	−6	12, 6, 2
		3	4, 3, 2				12		20, 12, 6
1	2	2	3, 2, 1	2	6	16	6	4	12, 6, 2
		1	2, 1, 0				2		6, 2, 0
		2	3, 2, 1				6		12, 6, 2
1	1	1	2, 1, 0	2	2	8	2	0	6, 2, 0
		0	1				0		2
1	0	1	2, 1, 0	2	0	4	2	−2	6, 2, 0
0	2	2	3, 2, 1	0	6	12	6	6	12, 6, 2
0	1	1	2, 1, 0	0	2	4	2	2	6, 2, 0
0	0	0	1	0	0	0	0	0	2

[a] $S_{24} = S_2 + S_4$, $S_{35} = S_3 + S_5$, $S_T = S_1 + S_{24} + S_{35}$. $S_1 = S_2 = S_3 = S_4 = S_5 = 1$.

Hence, the analytical form of the Hamiltonian is

$$H = a_0 + a_1 C_1 + a_2 {b_0}^2 + a_3(b_0 b_1) + a_4(S_1 + b_0)^2 + a_5(S_1 b_1) \qquad \text{(A5)}$$

where

$$a_0 = 4J_3 + 4J_2 + J_4 + J_5$$

$$a_1 = -{}^1/_4 J_3 - {}^1/_4 J_2 + {}^1/_2 J_1$$

$$a_2 = -J_1 + {}^1/_2 J_4 + {}^1/_2 J_5$$

$$a_3 = -{}^1/_2 J_3 + {}^1/_2 J_2$$

$$a_4 = -{}^1/_2 J_4 - {}^1/_2 J_5$$

$$a_5 = -J_4 + J_5$$

It is clear that the spin Hamiltonian in eq A5 contains Casimir operators of the algebra A1—the only exception being that of the last term—or scalar products of operators for which the eigenvalues can be evaluated easily. The last term of the spin Hamiltonian is the only scalar product affording nonzero off-diagonal matrix elements and can be treated by the perturbation theory.

There is a total degeneracy of $(2S + 1)^5 = 243$ and 51 different electronic levels for each pentamer, and the eigenvalues of each level can be calculated; see Table A1 and eq A5.

Supporting Information Available: Tables of χ_M and $\chi_M T$ for **1** and **2**, and the EPR spectra of both complexes (7 pages). Two X-ray crystallographic files, for complexes **1**·4Me_2CO·0.5C_6H_{14} and **2**·4Me_2CO, in CIF format, are available. Ordering and access information is given on any current masthead page.

IC9714091